CrossMark
click for updates

View Article Online
View Journal

Journal of
Materials Chemistry A

Accepted Manuscript

This article can be cited before page numbers have been issued, to do this please use: Y. Hao, X. Dong, X. Wang, S. Zhai, H. Ma and X. Zhang, *J. Mater. Chem. A*, 2016, DOI: 10.1039/C6TA02371A.

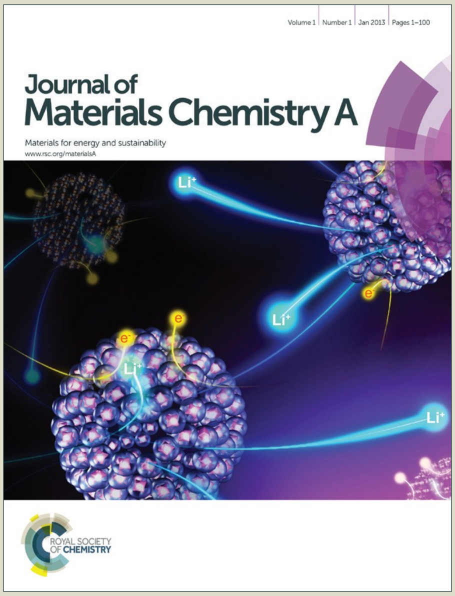
Volume 1 | Number 1 | Jan 2013 | Pages 1–100

Journal of
Materials Chemistry A

Materials for energy and sustainability
www.rsc.org/materialsA

ROYAL SOCIETY OF CHEMISTRY

This is an *Accepted Manuscript*, which has been through the Royal Society of Chemistry peer review process and has been accepted for publication.

Accepted Manuscripts are published online shortly after acceptance, before technical editing, formatting and proof reading. Using this free service, authors can make their results available to the community, in citable form, before we publish the edited article. We will replace this *Accepted Manuscript* with the edited and formatted *Advance Article* as soon as it is available.

You can find more information about *Accepted Manuscripts* in the Information for Authors.

Please note that technical editing may introduce minor changes to the text and/or graphics, which may alter content. The journal's standard Terms & Conditions and the Ethical guidelines still apply. In no event shall the Royal Society of Chemistry be held responsible for any errors or omissions in this *Accepted Manuscript* or any consequences arising from the use of any information it contains.

ROYAL SOCIETY
OF CHEMISTRY

www.rsc.org/materialsA

View Article Online
DOI: 10.1039/C6TA02371A

Journal Name

ARTICLE

Controllable electrostatic self-assembly of sub-3-nm graphene quantum dots incorporated into mesoporous Bi_2MoO_6 frameworks: efficient physical and chemical simultaneous co-catalysis for photocatalytic oxidation

Received 00th January 20xx,
Accepted 00th January 20xx

DOI: 10.1039/x0xx00000x

www.rsc.org/

Yuchen Hao, Xiaoli Dong*, Xiuying Wang, Shangru Zhai, Hongchao Ma and Xiufang Zhang

Over the past few years, the direct assembly of co-catalyst/modification material into mesoporous photocatalysts has been considered as a great challenge. Additionally, for photooxidation, the simultaneous achievement of fast charge separation, broad spectrum photocatalytic activity, higher carrier utilization efficiency (generating more active oxidizing groups) is quite necessary but has never been studied. To this end, we report here, for the first time, using sub-3-nm GQDs as co-catalyst, successfully achieved the uniform modification for mesoporous photocatalyst (mesoporous Bi_2MoO_6) by a novel electrostatic self-assembly method. The sub-3-nm GQDs, which were prepared from graphene nanosheet by a modified chemical oxide method, exhibit many unique physical and chemical properties, such as small size, electronic capture, up-conversion, especially peroxidase-like activity. After GQDs modified, the resulting mesoporous hybrid photocatalyst (GQDs-BM) exhibited excellent charge separation efficiency and broad spectrum photocatalytic activity from UV to NIR light. More importantly, we found that a certain amount of H_2O_2 was produced through the photoreduction effect in photocatalytic process. Unfavorably, for bare Bi_2MoO_6, the continuous-accumulating H_2O_2 could not efficiently convert into ·OH by one-photoelectron reduction, which means the indirect waste of photo-excited electrons. However, the chemical co-catalysis of GQDs could make this process ($H_2O_2 \rightarrow \cdot OH$) more quickly and efficiently, moreover, did not need any additional photoelectron, which means the effectively enhancement of the utilization efficiency of photo-excited electrons (generating more ·OH). Additionally, for the as-prepared GQDs-BM, the sharp increased photo-degradation activity for different target pollutants, such as BPA, MB, TC, CIP and phenol further confirmed that the physical and chemical simultaneous co-catalysis of GQDs can efficiently enhance the photocatalytic activity of mesoporous Bi_2MoO_6.

1. Introduction

Semiconductor photocatalysis has attracted worldwide attention for many years as an effective pathway to solve environment deterioration.[1-9] Specifically, photooxidation can provide an simple and low-cost way to achieve the destruction of toxic organic pollutants. Among various of photocatalysts, bismuth molybdate (Bi_2MoO_6), stable, innoxious and with a smaller band gap (2.5-2.8eV), has been considered as a promising candidate in organic dyes degradation and water splitting.[10-15] Specially, mesoporous Bi_2MoO_6, owing to its large surface-to-volume ratios and abundant porous structure, exhibits excellent optical absorption ability and surface catalytic activity.[16-20] But, to further optimize its photocatalytic performance, some modification are quite necessary.[21-23] However, difference from other bulk or sheet photocatalyst, mesoporous photocatalyst, which possesses abundant inner porous structure is very difficult to achieve fully surface contact with other materials. Specifically, for constructing nanocomposites or heterostructure, some modification materials, such as 2D graphene[24], Ag_2S[25], ZnO[26], C_3N_4[27-28], can only contact with the outside surface of mesoporous materials, but cannot be completely deposited into the porous channel, and very difficult to achieve fully dispersion within it. In this article, using mesoporous Bi_2MoO_6 as counterpart, we report a smart way to achieve the uniform modification for mesoporous photocatalyst by utilizing ultrasmall 0D-sized quantum dots as co-catalyst.

To enhance photocatalytic activity, referring existing research results, two main strategies can be presented which mainly belong to physics: (i) enhancing optical absorption; (ii) suppressing charge recombination.[29-32] Specifically, although the mesoporous structure can enhance light absorption ability, but the optical window cannot be efficiently expanded.[33-34] Accordingly, broadening optical spectrum and making the photocatalyst possesses broad spectrum photocatalytic activity form UV to Near-Infrared light is quite

---

School of Light Industry and Chemical Engineering, Dalian Polytechnic University, #1 Qinggongyuan, Dalian 116034, P R China E-mail: dongxiaoli65@163.com
Electronic Supplementary Information (ESI) available: [details of any supplementary information available should be included here]. See DOI: 10.1039/x0xx00000x

View Article Online
DOI: 10.1039/C6TA02371A

necessary. Besides that, the mesoporous photocatalysts possess large surface area, which not only can provide more activity sites but also means more surface trapping states, leading to surface carrier recombination, so, constructing a nanocomposite and achieving the fast transfer of photo-generated carriers is also very important.[35-36] However, to the best of our knowledge, simultaneously achieved above two aspects is still possesses challenges.

For photocatalytic oxidation, besides light absorption and carrier separation, the conversion from photo-generated carriers to strong oxidizing groups is also very important but lack of attention. As is known, the essence of photooxidation is utilizing strong oxidizing groups (such as ·OH, $\cdot O_2^-$) and holes to achieve the oxidation of pollutants (such as dye, BPA, MB), which means if a fixed number of photo-excited carriers can generate more strong oxidizing groups, the oxidation ability of photocatalyst will be further enhanced, leading to excellent photooxidaiton activity.[37-42] Difference from holes, the photo-excited electrons do not possess oxidation ability, and, as a multi-electron reduction reaction ($2H^+ + O_2 + 2e^- \rightarrow H_2O_2 + e^- \rightarrow \cdot OH + OH^-$), the conversion from electrons to oxidizing groups is quite complex.[43-44] Additionally, in this work, we found that a certain amount of H_2O_2 can be produced through the photoelectron reduction reactions, but, for bare Bi_2MoO_6, these photogenerated H_2O_2 constantly accumulate and cannot efficiently convert into strong oxidizing groups (·OH), which means the indirect waste of photo-excited electrons (generating H_2O_2). It was hypothesized that, if a novel chemical co-catalysis can achieve the effective and quick conversion from photogenerated H_2O_2 to ·OH, even do not need additional photo-excited electrons, the photo-excited electrons will generate more oxidizing groups (·OH), which is beneficial for further enhancing the photooxidation activity compared with only physical co-catalysis.

Graphene quantum dots (GQDs), a graphene based material with size less than 10nm, has attracted increasing attention owing to its unique physical and chemical properties.[45-48] Specifically, in photocatalytic fields, the electrical conductivity of GQDs has been considered as an efficient way to suppress carrier recombination.[49] But, the systematically study of utilizing the up-conversion property of GQDs to broaden the optical window of photocatalyst was still absent. Moreover, GQDs also possess high chemical catalysis activity (peroxidase-like activity), which can catalyze the decomposition of H_2O_2, generating ·OH under dark.[50] And this property can provide a new direction to enhance the photooxidation performance by the chemical co-catalysis which is proposed for the first time in this article.

Herein, for the first time, using mesoporous Bi_2MoO_6 as counterpart, sub-3-nm GQDs as co-catalyst, we provided a novel electrostatic self-assembly method to achieve the incorporation of ultrasmall GQDs into mesoporous Bi_2MoO_6 frameworks (GQDs-BM). More importantly, the mechanism of the physical (electronic capture and up-conversion property) and chemical (peroxidase-like activity) co-catalysis of GQDs have been systematically investigated in this paper. Moreover, the photodegradation experiments of various target pollutants further ensured that the GQDs as co-catalyst can efficiently enhance the photooxidation activity of mesoporous bismuth molybdate. We believe, our work can provide a smart way to modify mesoporous photocatalyst using ultrasmall OD-sized material as co-catalyst, and facilitate the utilization of GQDs as co-catalyst in photocatalytic fields.

2. Experimental

Synthesis of hierarchical mesoporous Bi_2MoO_6 hollow (M-BM)

In a typical procedure, 242 mg $Bi(NO_3)_3{\cdot}5H_2O$ and 60 mg $Na_2MoO_4{\cdot}2H_2O$ were dissolved in 10 mL of ethylene glycol (EG) respectively under magnetic stirring. After completely dissolved, the two solutions were mixed together, then the mixture solution were dropwised into 30 ml isopropanol, follow by stirring for 20 min, and the resulting solution was transferred into a 50 mL Teflon stainless steel autoclave, and heated to 160 °C for 24 h. After the autoclave was air-cooled to room temperature, the mixture was centrifugaled, washed with distilled water and ethanol, and dried at 80 ^oC in air.

Synthesis of sub-3-nm ox-GQDs

200 mg of graphite oxide (synthesized through chemical exfoliation of graphite powders using a modified Hummers' method[51-52]) were dispersed in 500 mL of deionized water and ultrasound (200 W, 40 kHz) for 2.5 h, the mixture was centrifuged at 6000 rpm to collect the supernatant liquid and vacuum drying to obtain small size graphene oxide sheets. Then, 30 mL as-prepared small size graphene oxide sheets solution (0.5mg/mL) was first mixed with 8 ml concentrated nitric acid and 3 mL sulphuric acid, after ultrasound for 1h, the mixture was then transferred to a 100 ^oC oil bath and stirred for 24 h. After cooling to room temperature, the mixture was placed under the mild ultrasonication for 20 min. Then sodium carbonate (Na_2CO_3) was added to the mixture solution until pH=8. Finally, the mixture were filtered through a 0.22μm microporous membrane and the final product solution was further dialyzed in a dialysis bag (retained molecular weight: 1000 Da), and light yellow solution of ox-GQDs were obtained.

Fabrication of GQDs-BM nanocomposite

The GQDs/M-Bi_2MoO_6 hybrid (GQDs-BM) was prepared through a surface charge modification method and a simple hydrothermal treatment. The M-BM powders were functionalized by APTES. Briefly, 0.5 g of M-BM powder was dispersed in 250 mL of ethanol and ultrasound for 30 min. Next, 1.6 mL of APTES was added, and the mixture solution was treated in refluxing ethanol solution under 70 °C for 4 h. After that, the powder was collected, washed with ethanol and water three times, respectively. After dried at 60 °C in air, 0.4 g of as-prepared APTES-modified M-BM was added into 32 mL of deionized water and ultrasound for 20 min. 8 mL of the as-synthesized ox-GQDs solution (1mg/mL) were added to the as-obtained M-BM suspension and stirred for 2 h, follow by ultrasound for 30 min. The suspension was then transferred to a Teflon-sealed autoclave and maintained at 180 ^oC for 6 h to achieve GQDs-BM hybrid material. Finally, obtained products were collected, washed with water, and freeze drying.

Characterization and measurements

The TEM analyses were performed by a JEOL JEM-2100F transmission electron microscope. SEM images were taken using a field-emission scanning electron microscope (JSM-7800F, JEOL). The crystallinity and the purity of the as-prepared samples were

View Article Online
DOI: 10.1039/C6TA02371A

characterized by powder X-ray diffraction (XRD) analysis on a Shimadzu XRD-6100 diffractometer at 40 kV and 40 mA with Cu Ka radiation. Data were recorded at a scan rate of 0.07°/s in the 2Theta range 10^{o}-70^{o}. X-ray photoelectron spectroscopy (XPS) measurement by a Thermo VG ESCALAB-250 system with Al-Kα and Mg-Kα source operated at 15 kV. Light absorption property was evaluated by UV-vis diffuse reflectance spectra (UV-vis DRS, CARY 100&300, VARIAN), $BaSO_4$ was used as a reflectance standard. The PL spectra of the photocatalysts were analysis using Hitachi F-7000 fluorescence spectrophotometer. The N_2-sorption measurement was performed by using Micromeritics Tristar 3000 at 77 K, the poresizedistribution were estimated using the Barrett-Joyner-Halenda (BJH) methods.

Electrochemical and photocatalytic test

Photoelectrochemical measurements were carried out on a CHI660E electrochemical workstation (Shanghai Chenhua, China) using a three-electrode configuration with the as-prepared samples as working electrodes. The working electrodes were prepared by dip-coating method, 5 mg of sample was suspended in 0.15 mL of ultrapure water to produce slurry, which was then dip-coated onto a glass carbon electrode and dry under an alcohol environment. All investigated electrodes show a similar thickness. The light source is a 300 W Xe lamp (PLS-SXE 300, Beijing Perfect Light Co., Ltd.). The current J-V curves of the working electrodes were obtained by the linear sweep voltammogram (LSV) with a scan rate of 10 mV/s. The photocurrent response was obtained by potentiostatic (current vs. time, I-t) measurements under intermittent illumination at a bias of 0.7 V vs. SCE. Electrochemical impedance spectroscopy (EIS) was conducted with an alternating current signal (10mV) in the frequency range of 0.1-10^{5}Hz at open circuit potential (OCP). Mott-Schottky plots were measured at a frequency of 100 Hz in the dark. The incident photon to current conversion efficiency (IPCE) was calculated by the following formula.

$$IPCE(\lambda) = \frac{1240\, j(\lambda)}{E(\lambda)\lambda} \times 100$$

Where λ is the wavelength (nm), j is the photocurrent density, and E is the incident power of the monochromatic light. The E was measured with a photometer, and the photocurrent density (j) was determined by measuring current versus time curve at a constant potential (1.0 V_{SCE}).

Photocatalytic activity measurements

The photocatalytic performance were evaluated by the decomposition of RhB, bisphenol A (BPA), ciprofloxacin (CIP), tetracycline hydrochloride (TC), methylene blue (MB) and phenol under simulated sunlight irradiation. And the pH value was not adjusted when the reaction was conducted. The light source for photocatalytic reaction was a 300 W Xe lamp (PLS-SXE 300, Beijing Perfect Light Co., Ltd.). The distance between the Pyrex glass and the light source was about 10 cm. The photocatalytic activity of the prepared catalysts under simulated sunlight was estimated by measuring the degradation rate of RhB (10 mg/L), BPA (10 mg/L), CIP (10 mg/L), TC (10 mg/L), MB (10 mg/L) and phenol (10 mg/L) in an aqueous solution. Specifically, 0.2 g/L photocatalyst were added in quartz reactor which contained 50 mL pollutants aqueous solution. Before irradiation, the mixture was stirred in the dark for 45 min to ensure the absorption-desorption equilibrium between the model pollutants and the photocatalyst. In the process of photocatalytic degradation, a certain volume of suspension (about 3 mL) was sampled every 10 min, then centrifuged immediately to remove the particles. The filtrates were analyzed for residual pollutants concentration, the absorbance was measured by UV-vis spectrophotometer and normalized concentration changes (C/C_0) of RhB, BPA, CIP, TC, MB and phenol were obtained based on the maximum absorption at 554 nm, 278 nm, 276 nm, 356 nm, 664 nm and 268 nm, respectively.

3. Results and discussion

3.1 Co-assembly process and morphological studies.

In the co-assembly process, to ensure the sub-3-nm GQDs can uniformly and stably deposited on the outside surface/inner channels of mesoporous Bi_2MoO_6 (M-BM), two mainly strategies were proposed: (i) ultrasound-assisted dipping; (ii) electrostatic self-assembly. Specifically, the mesoporous Bi_2MoO_6 (M-BM) was prepared via a solvothermal approach, after being modified with APTES, the surface of M-BM holds amine functional groups which were positively charged. Additionally, the ox-GQDs synthesized from GO nanosheet were negatively charged. Through the ultrasound-assisted dipping process, the ox-GQDs solution fully entered into the channels and achieved sufficient contact with M-BM, afterwards, under the effect of electrostatic attraction, the ox-GQDs were driven and anchored on the surface of M-BM. And finally, the ox-GQDs were reduced to the GQDs through hydrothermal effect, and the GQDs-BM hybrid was successfully obtained (see Scheme 1). Compared with physical mixture, the electrostatic self-assembly can make the GQDs contact with M-BM more fully, and enhance the stability of GQDs-BM hybrid, leading to more excellent photooxidation performance (Fig. S1). Moreover, the optimal loading level was investigated by the photodegradation experiments with different samples as photocatalyst (Fig. S2).

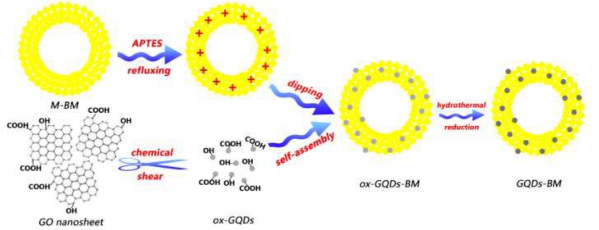

Scheme 1. The schematic diagram of the co-assembly process.

The high-magnfication SEM image of GQDs-BM hybrid material (Fig. 1a) can help us to observe subtle structure. It clearly shows that the hollow sphere was consisted of many nanosheets which were of several nanometers in thickness. The cross-linking of nanosheets formed hierarchical flower-like mesoporous spheres (the mesoporous structure of GQDs-BM is supported by the nitrogen sorption isotherms and pore size distributions curves, Fig. S3). And we can easily obtain that the spheres have hollow structure and the shell thickness is about 200 nm. Moreover, the EDX elemental mapping results (Fig. S4) reveal an uniform

View Article Online
DOI: 10.1039/C6TA02371A

distribution of C, O, Mo and Bi elements throughout the material, suggesting the successful deposition of GQDs on the surface of M-BM. Fig. 1b shows one complete hollow sphere of GQDs-BM hybrid, it can clearly reveals that many nanosheets reciprocal chiasma form 3D mesoporous hierarchical structure and an obvious contrast between the dark edge and the bright center confirmed their hollow structure. Fig. 1c and d shows the deposition of GQDs on mesoporous Bi_2MoO_6, many ultrasmall black spots (sub-3-nm) not only deposited on the external surface of mesoporous Bi_2MoO_6, but also inner the porous channels, indicative of the formation of GQDs-BM hybrid material (also shown in Fig. S5). The better deposition of GQDs on M-BM can be interpreted as the sufficient dipping process and the electrostatic interaction effect. As shown by the HETEM image (inset, Fig. 1c), we can easily find two different lattice distance of 0.23 nm and 0.31 nm, which can be attributed to the (200) spacing of GQDs and (131) spacing of Bi_2MoO_6.

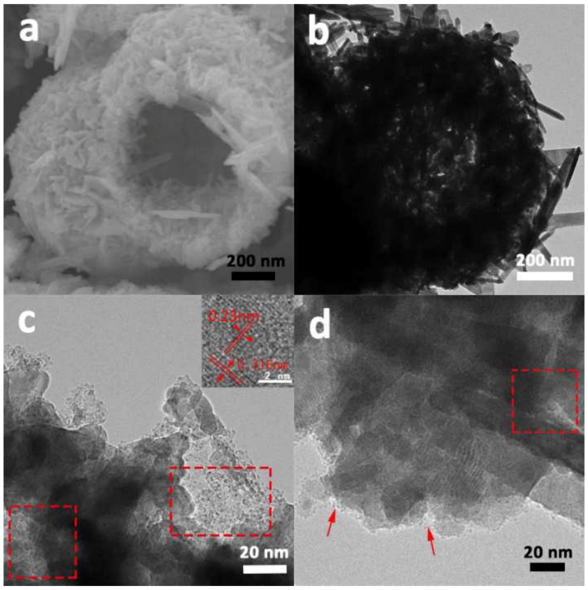

Fig. 1 (a) SEM image, (b)-(d) TEM images and HRTEM image (inset in Figure (c)) of prepared GQDs-BM hybrid material.

3.2 Phase and chemical composition

We performed XRD analysis to determine the structural phases of as-prepared GQDs-BM hybrid and M-BM. For Fig. 2a, the distinct diffraction peaks of different samples at 28.3°, 32.9°, 47.0°, 56.0°, 58.5°, and 68.8° corresponding to (131), (002), (062), (133), (262), and (400) crystal planes of orthorhombic Bi_2MoO_6 (JCPDS 84-0787), respectively. As expected, after the deposition of GQDs, a very weak diffraction peak around 24.7° which belong to GQDs can be found, indicating that the GQDs-BM hybrid was successfully synthesized.[53-55] Additionally, no other diffraction peaks from impurities can be found, indicating the as-prepared samples possess high purity.

The samples were further characterized by Raman spectrum. As indicated in Fig. 2b, for GQDs-BM and M-BM, the obvious peaks at 294, 344, 808 and 844 cm^{-1} can be considered from pure Bi_2MoO_6. But for GQDs-BM and bare GQDs, the G band peak of the GQDs at 1590 cm^{-1} are related to the E2g vibrational mode of aromatic domains in the two-dimensional hexagonal lattice structure. The amorphous D band peak appeared at 1370 cm^{-1}, with an I_D/I_G ratios about 0.97, which is similar with previous work.[56-57] Besides that, for FT-IR spectrum (Fig. 2c), the absorption bands at 567 cm^{-1} and 734 cm^{-1} can be considered as the asymmetric stretching mode and the bending vibration of the MoO_6, the absorption band at 842 cm^{-1} be identified based on asymmetric and symmetric vibration modes (Mo-O stretching) of the corner sharing $(MoO_6)^{6-}$ octahedron which can prove existence of pure Bi_2MoO_6. For the GQDs-BM hybrid and bare GQDs, the existence of C-O stretching peak at 1120 cm^{-1}, C-H bending peak at 1390 cm^{-1} and a weak absorption of C=O vibrational stretch was observed at 1726 cm^{-1} belong to GQDs, which can also ensure the successfully synthesis of GQDs-BM hybrid photocatalyst.

Moreover, to further to identify the surface chemical composition of M-BM and GQDs-BM hybrid photocatalyst, and the interaction between M-BM and GQDs, the XPS analysis was performed. Specifically, for high-resolution C1s spectrum (Fig. 2d), the peak at 284.2 eV corresponds to the C-C coordination with sp^2 orbital and the peak at 286.2 eV belongs to the C-O coordination of GQDs. The weaker peaks around 287.5 eV (C=O) and 290 eV (-COOH) belong to the surface functional groups of GQDs.[58-60] Furthermore, the high-resolution Bi 4f spectrum (Fig. S7a) exhibits obvious peaks at 158.0 eV ($Bi4f_{7/2}$) and 162.9 eV ($Bi4f_{5/2}$), ascribed to the Bi^{3+} in crystal structure. Additionally, after the deposition of GQDs, the Bi4f peak exhibits an obviously shift compared to the Bi 4f peak of bare M-BM, which indicates that the surface chemical environment in GQDs-BM hybrid has changed.[61] The Mo3d peaks are centered at 232.4 eV and 235.5 eV are ascribed $Mo3d_{5/2}$ and $Mo3d_{3/2}$, respectively (Fig. S7b). The high-resolution O1s spectrum (Fig. S7c) shows three different peaks at 530 eV, 531.8 eV and 532.8 eV which belong to the lattice oxygen in crystalline Bi_2MoO_6, C-O and C=O groups from GQDs, respectively. The XPS analysis indicates the codependent of GQDs and M-BM, which is consistent with the Raman spectrum and FT-IR analysis.

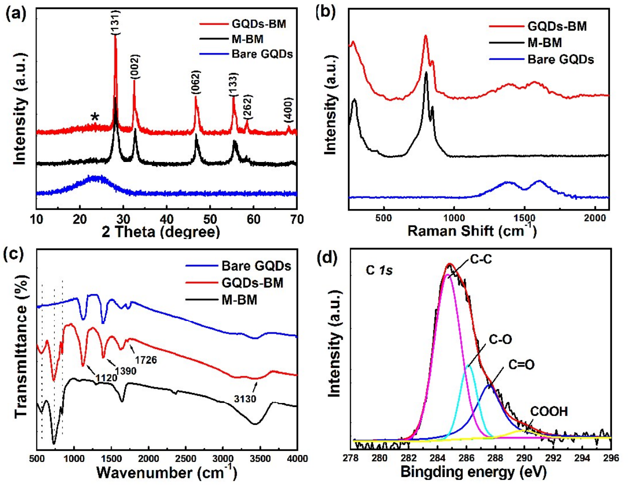

Fig. 2 (a) XRD patterns (b) Raman spectrum (c) FT-IR spectrum of GQDs-BM, M-BM and bare GQDs; (d) high-revolution C1s XPS spectrum of GQDs-BM hybrid. Note that the Raman spectrum of GQDs-BM and GQDs was obtained by deducting the background of GQDs owing to its strong photoluminescence effect during characterization.

View Article Online
DOI: 10.1039/C6TA02371A

3.3 Investigating the physical co-catalysis of GQDs

3.3.1 Suppressing surface recombination

The suppression of surface charge recombination by the electronic capture effect of GQDs were investigated through photoluminescence spectrum (PL), electrochemical impedance spectroscopy (EIS), transient photocurrent (I-T) and IPCE curves. From PL spectrum (Fig. 3a), the GQDs-BM hybrid and M-BM exhibit strong emission peak at approximately 472 nm, which is mainly assigned to the emission of the band-gap transition. By contrast, we can easily obtain that the weaker peak intensity around 472nm for GQDs-BM which indicates higher carrier separation efficiency.[62-63] Additionally, through EIS spectrum we can profound insights into the carrier transport in the heterojunction system.[64-65] The radius of each arc on the EIS Nyquist plot reflects the charge transfer process occurring at the contact interface between the electrode/electrolyte interface, and the smaller radius represents the lower charge transfer resistance. So, the GQDs-BM hybrid exhibits smaller charge transfer resistance compare with M-BM (Fig. 3b). Suggesting that the GQDs-BM hybrid exhibits faster interfacial charge transfer between the electrode and electrolyte after the GQDs deposited, which mainly due to the effective separation of photo-generated electron-hole pairs. As is known, considering the surface charge recombination, the carrier separation efficiency can takes into account efficiencies for two fundamental processes which can be expressed by Eq. 1.

$$\eta = \eta_{sep} \times (1 - \eta_{rec}) \qquad (1)$$

Where η is the total carrier separation efficiency, η_{sep} is the bulk carrier separation efficiency (inner the photocatalyst), and η_{rec} is the surface charge recombination rate. Considering the deposition of GQDs cannot change the morphological structure and essential attribute of matrix material (mesoporous Bi_2MoO_6), the bulk carrier separation efficiency (η_{sep}) before and after GQDs deposited nearly the same. Consequently, the PL and EIS spectrum can indirect indicate that the GQDs-BM hybrid exhibits less surface recombination.

For deepen understanding the role of GQDs for promoting carriers separation, we investigated the surface recombination process in M-BM and GQDs-BM photocatalyst.[66-67] Transient photocurrent is a good tool to gain information on surface recombination process. From Fig. 3c we can clearly obtain that the photocurrent transient of M-BM is much more conspicuous than that of GQDs-BM, which means more surface carrier recombination in M-BM than that in GQDs-BM. Furthermore, by comparing the incident photon to current conversion efficiency (IPCE) before and after GQDs loaded, we also obtain that the deposition of GQDs can effectively suppressing the surface recombination. Specifically, in Fig. 3d, the IPCE of M-BM is far less than that of GQDs-BM hybrid. However, an obvious improvement of IPCE performance of M-BM is observed (Fig. 3e) after decoupling surface recombination by adding the hole scavenger Na_2SO_3 (in the presence of which surface recombination is suppressed due to its rapid and facile oxidation[36]). However, the IPCE of GQDs-BM only changed a little, which means the GQDs played the same role as Na_2SO_3: suppressing surface recombination. Accordingly, the GQDs as electron traps can efficiently suppress surface charge recombination, which is beneficially for enhancing the photocatalytic performance of mesoporous photocatalyst.

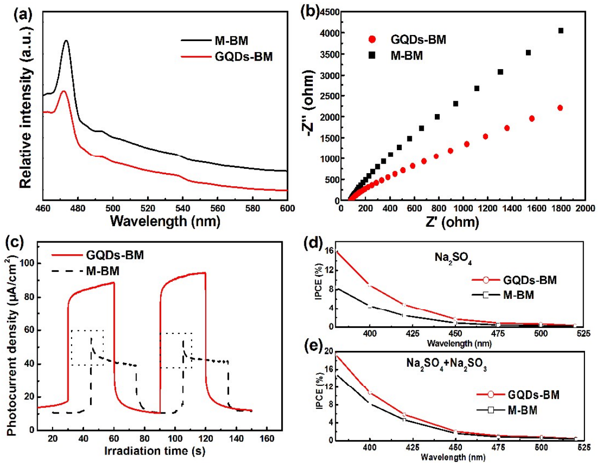

Fig. 3 Photoluminescence (PL) spectra (a), EIS Nyquist plots (b), transient photocurrents versus time plotted (c), incident photon to current conversion efficiency plotted was measured in 0.5M Na_2SO_4 solution (d), 0.5 M Na_2SO_4 solution together with 0.5M Na_2SO_3 solution as hole-capture (e) of as-prepared GQDs-BM and M-BM.

3.3.2 Broadening optical window

The optical absorption of M-BM and GQDs-BM hybrid were investigated by DRS spectrum (Fig. 4a). The absorption edge of the M-BM was about 480nm, indicating that the M-BM can only harvest little scope of visible light which agrees with the previous report.[68] But, after the GQDs deposited, the light absorption ability obviously enhanced (UV light), which is beneficial for the light harvesting. However, more importantly, the optical window of photocatalyst further broadened which mainly owing to the up-conversion property of GQDs. Specifically, from the DRS spectrums of bare GQDs (Fig. S9b) and GQDs-BM hybrid, an obvious absorption peak from 600 nm to 800 nm can be found, which means GQDs-BM hybrid can achieve the absorption of long-wavelength visible light and NIR light after GQDs deposited. Furthermore, the up-conversion property of GQDs can be evidenced by PL emission. As shown in Fig. 4b, the strong emission peaks of GQDs in the range of 350 to 500nm which was motivated with 660 nm to 780 nm light can be found. It is indicate that the GQDs exhibit excellent up-conversion property which can achieve the conversion from NIR light to visible light. Besides that, to investigate the effect of up-conversion property on the practical photocatalytic performance, the J-V curves and photodegradation curves under 650nm-cut simulated sunlight were obtained. The J-V curve of different samples clearly reveals that the GQDs-BM hybrid exhibits a significant photocurrent response, but, for bare M-BM, no obvious photocurrent response can be found (Fig. 4c). This phenomenon clearly indicates that the GQDs-BM hybrid can utilize long-wavelength/NIR light to produce active electrons and holes. Moreover, the broad spectrum photocatalytic activity is also supported by the obvious photodegradation performance of GQDs-

View Article Online
DOI: 10.1039/C6TA02371A

BM hybrid under 650nm-cut simulated sunlight (Fig. 4d), which can decompose 28% of pollutants (BPA) within 140 min. In summary, the GQDs as co-catalyst can absorb long-wavelength/NIR light and convert it to visible light, which can be utilized by mesoporous Bi_2MoO_6 to produce photogenerated carriers and achieve the photodegradation of pollutants.

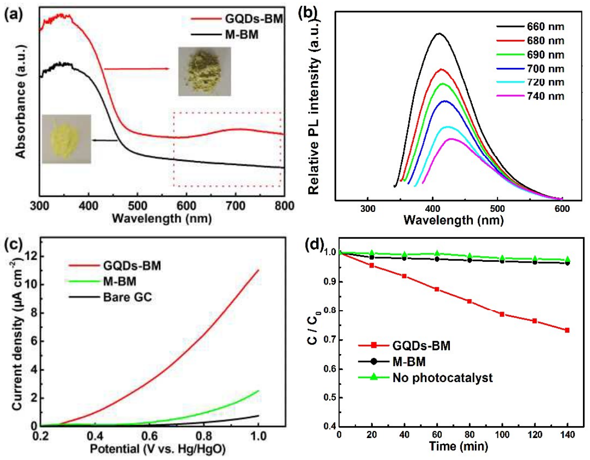

Fig. 4 (a) UV-vis absorption spectra of M-BM and GQDs-BM (red curve) catalysts and digital photograph of catalyst grains (inset); (b) up-conversion PL spectra of GQDs under different excitation wavelength; J-V curves (c) and photodegradation curves (d) of different samples under 650nm-cut simulated sunlight.

3.4 Investigating the chemical co-catalysis of GQDs

The specific peroxidase-like activity of GQDs can create possibility for further enhancing the conversion efficiency from photo-excited electrons to strong oxidizing groups (·OH), leading to more excellent photocatalytic oxidation activity of hybrid photocatalyst. From Mott-Schottky plot (Fig. 5a), we can obtain that the flat band potentials (V_{fb}) of M-BM is about 0.01 V *vs.* NHE. And the conduction band position of M-BM is estimated to be -0.09 V *vs.* NHE because the conduction band edge is generally more negative by -0.1 V than V_{fb} for n-type semiconductor.[69] This values of E_{CB} is similar with the one-electron reduction potential of O_2 ($E_o(O_2/\cdot O_2^-)$ = -0.057 V vs NHE) and more negative than two-electron reduction of O_2 ($E_o(O_2/H_2O_2$ = 0.70 V vs NHE).[70,44] Consequently, for bare M-BM and GQDs-BM hybrid, in the process of photocatalytic, the photo-generated electrons can generate some $\cdot O_2^-$ by reducing O_2 (Eq. 2). Besides that, some H_2O_2 also can be produced by two main routes which are one-electron reduction of $\cdot O_2^-$ (Eq. 3) and two-electrons reduction of O_2 (Eq. 4).[71-74] This conclusion can be supported by Fig. 5b, which examined the possible formation of H_2O_2 by a colorimetric DPD method.[75] When using bare M-BM as photocatalyst, the photogeneration of H_2O_2 was very obvious, and with the increases of reaction time, the production of H_2O_2 increased consecutively. On the other hand, for bare M-BM, the generated H_2O_2 can transformed into ·OH by trapping one electron (Eq. 5)[43], but, the continuous accumulation of H_2O_2 indicates that this process was very inefficient, which means the indirect waste of photoelectrons (generating H_2O_2). However, after GQDs deposited, the H_2O_2 detected in the photodegradation process was very little, and did not found obvious accumulation. On the basis of experimental, we can suggest that the photogenerated H_2O_2 can be quickly decomposed by the co-catalysis of GQDs.

$$O_2 + e^- \rightarrow \cdot O_2^- \qquad (2)$$

$$\cdot O_2^- + e^- + 2H^+ \rightarrow H_2O_2 \qquad (3)$$

$$O_2 + 2H^+ + 2e^- \rightarrow H_2O_2 \qquad (4)$$

$$H_2O_2 + e^- \rightarrow \cdot OH + OH^- \qquad (5)$$

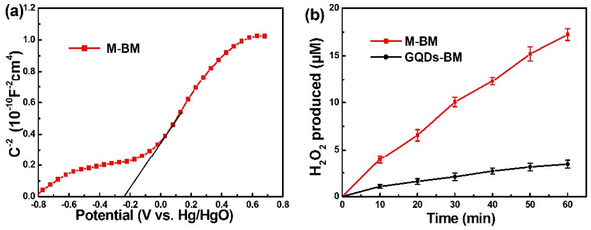

Fig. 5 (a) Mott-Schottky plot of as-prepared M-BM, (b) production of H_2O_2 under simulated sunlight irradiation (in the presence of BPA as pollutant).

In order to further confirmed the catalyst activity of GQDs for H_2O_2 decomposition, the electrochemical behavior of different work electrodes made by M-BM, GQDs and GQDs-BM were measured using Linear sweep voltammetry (LSV) in PBS buffer solution containing H_2O_2 (Fig. 6a). We can clearly obtain that the GQDs-BM and GQDs work electrodes exhibit higher reduction current density, which means both GQDs-BM hybrid material and GQDs possess strong catalytic activity toward H_2O_2 decomposition. Comparing the lower current density of M-BM, we can also suggest that the deposition of GQDs can make the hybrid material exhibit catalyst activity for H_2O_2. Furthermore, to explore the product of H_2O_2 catalytic decomposition, fluorescence experiments were taken to detect ·OH during the reaction. According to the previous research[50], Terephthalic acid (TA) was used as a fluorescence probe for tracking of ·OH because it could capture ·OH and generate 2-hydroxy terephthalic acid (TAOH), which emitted unique fluorescence around 435 nm. Fig. 6b shows the change of fluorescence intensity in the mixed solution of TA, H_2O_2 and GQDs, the presence of ·OH can be proved through found a remarkable fluorescence enhancement at 435 nm relative to control experiments after 2h reaction (the respectively PL intensity shown inner the Fig. 6b). The above experiments fully illustrates that the presence of ·OH during the catalytic decomposition of H_2O_2 by GQDs or GQDs-BM hybrid under dark.

To deep understand the contribution of peroxidase-like activity of GQDs and the coordination mechanism between M-BM and GQDs in the photooxidation process. The J-V curves of GQDs-BM hybrid and M-BM work electrodes in the ultrapure water without any other to add were conducted (Fig. 6c). It can clearly reveals that the GQDs-BM hybrid achieves a higher reduction current density (-0.71 mA/cm^2 -0.8V vs. SCE) which is about 3.2 folds larger than that of M-BM (-0.22 mA/cm^2 -0.8V SCE). The improvement of current density are more remarkable than that of oxidizing current density (about 2.2 times, Figure 3c), which indicates that part of photo-reduction reactions in GQDs-BM hybrid did not need photoelectrons. Considering the special chemical catalytic activity of GQDs for H_2O_2 decomposition, we can suggest that there are two types of reduction reactions occur on the surface of the GQDs-BM hybrid in the photocatalytic process: one is the photoelectrons participated, the other is the GQDs participated (no light is needed). To further verify the chemical co-catalysis of GQDs, single factor experiments were conducted which can efficiently avoid the interference from surface charge recombination and other factors such as light absorption performance. As is known, after the GQDs deposited, the higher light-harvesting performance and expanded optical window will make the hybrid photocatalyst generate more photoelectrons, so, to investigate the chemical co-catalysis of GQDs more accurate, the different photoelectric conversion performance should be avoided. To this end, firstly, the J-V plots of GQDs-BM and M-BM in ultrapure water without any other to add under monochromatic light were obtained (Fig. S10). Unlike above experiments, we use the relative current density which can estimate by dividing the current density by IPCE (in Na_2SO_4, no holes capture; Fig. 3d) to reflect the degree of reduction reactions on different samples. The Fig. 6d and e shows the relative current density under 380nm and 420nm monochromatic light, respectively. It can clearly reveals that the J/IPCE for GQDs-BM is about 1.4 times (380nm, -0.85 V vs. SCE) and 1.5 times (420 nm, -0.85V vs. SCE) higher than bare M-BM, which means more reduction reactions occurred on GQDs-BM surface. Similarly, using Terephthalic acid (TA) as fluorescence probe, the relative fluorescence intensity which obtained by dividing the fluorescence intensity (in ultrapure water contained 0.5M Na_2SO_3 as hole capture to avoid the interference from the ·OH produced by holes) by the IPCE (in Na_2SO_4 and 0.5M Na_2SO_3; Fig. 3e) under monochromatic light can be used to detect ·OH. Through the images inner the Fig. 6d and e, the ΔPL/IPCE for GQDs-BM is higher than M-BM, which means the GQDs-BM hybrid exhibits higher efficiency for generating ·OH by the chemical co-catalysis of GQDs. Moreover, Fig. 6f shows the PL intensity of GQDs-BM and M-BM at different reaction time in the whole photocatalytic process, we can obtain that the PL intensity of GQDs-BM is about 1.85 times higher than M-BM, which is more remarkable than the improvement of IPCE (Fig. 3e, about 1.25 times). Additionally, with the increases of reaction time, the PL intensity of GQDs-BM hybrid increased consecutively and did not reach saturation, which can indicates that the chemical co-catalysis of GQDs is stable, durable and high-efficiency.

In summary, after the deposition of GQDs, the photogenerated H_2O_2 can fully and efficiently convert into ·OH, which can avoid the indirect waste of the photo-excited electrons. Additionally, this chemical co-catalysis process do not need any photoelectrons, which means the photoelectrons reduction reaction from H^+ and O_2 to ·OH only need two photoelectrons (three photoelectrons before GQDs loaded). Moreover, in the photocatalytic process, the reduction of O_2 to H_2O_2 [$E_0(O_2/H_2O_2$ = 0.70 V *vs.* NHE)] and reduction of H_2O_2 to ·OH [$E_0(H_2O_2$/·OH) = 0.71 V *vs.* NHE] have similar standard redox potentials.[44] Then O_2 would compete with H_2O_2 for photoelectrons in photocatalytic process. But after the deposition of GQDs, it can quickly reduce H_2O_2 to produce ·OH but do not need photoelectrons, which means the competition between O_2 and H_2O_2 for photoelectrons will no longer exist. Accordingly, more photoelectrons will be used to produce H_2O_2 or $\cdot O_2^-$, and the as-generated H_2O_2 can be further convert into ·OH by the chemical co-catalysis of GQDs.

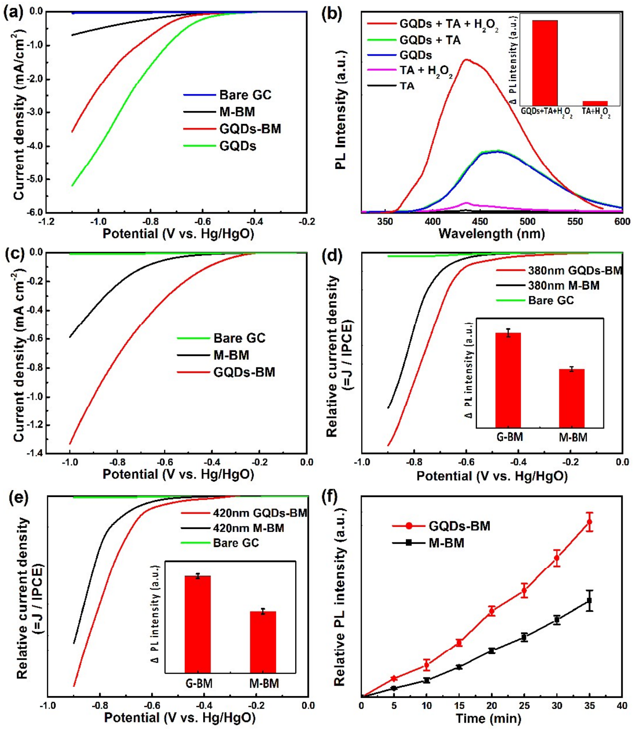

Fig. 6 (a) Current-potential plots for GQDs, GQDs-BM and M-BM in PBS buffer solution (PH=7.0) containing H_2O_2 (50 mM) in dark. The working electrodes were prepared by dip-coating, 20 μL GQDs solution (1mg/mL), GQDs-BM and M-BM solution (5 mg of sample was suspended in 0.15 mL of ultrapure water to produce slurry) was dip-coated onto glass carbon electrodes and dry under an alcohol environment, respectively. (b) Fluorescence spectra of the PBS solution (pH = 7.4) include only TA; TA and H_2O_2; only GQDs; TA and GQDs; TA, GQDs and H_2O_2 after 2 h reaction. The concentrations of TA, H_2O_2 and GQDs were 0.5 mM, 1 mM and 100 μg/mL, respectively. Histograms of relative PL intensity (inset) showed the catalysis effect of GQDs. (c) Current-potential plots for GQDs-BM and M-BM in ultrapure water without any other to add under the simulated sunlight. (d), (e) Relative current-potential plots for GQDs-BM and M-BM in ultrapure water without any other to add under 380nm and 420nm monochromatic light. Relative PL intensity (inset Fig. (d),(e)) in ultrapure water with 0.5M Na_2SO_3 solution as hole-capture and 0.5 mM TA as fluorescence probe under 380nm and 420nm light after 2 h reaction. (f) PL intensity-time plots for GQDs-BM and M-BM in ultrapure water with 0.5M Na_2SO_3 solution as hole-capture and 0.5 mM TA as fluorescence probe under simulated sunlight irradiation.

3.5 Photocatalysis mechanism, performance and stability

3.5.1 Active species trapping and photocatalysis mechanism

To determine the contribution of each active species in the photocatalytic system, trapping experiments were conducted. In the trapping experiment, different radical scavengers, such as ammonium oxalate (AO), *p*-benzoquinone (BQ) and *tert*-butanol (TBA) were added into the degradation system, respectively. As shown in Fig. S11, when TBA (·OH scavenger) was added, the photocatalytic oxidation rate was obviously decreased, which is more remarkable than other conditions. It is validating that the ·OH

View Article Online
DOI: 10.1039/C6TA02371A

play the most important role in the photooxidation process. Additionally, after AO (h^+ scavenger) added, the photo-degradation rate was apparently decreased, which means that the h^+ also play important role in the photoreaction process. Moreover, after BQ ($\cdot O_2^-$ scavenger) was added, the photodegradation rate was decreased but not obvious. By contrast, we can suggest that the ·OH were not only generated by the oxidation of OH^-, but also produced by the reduction of H_2O_2.

Basis on the experimental, the schematic elaboration of photocatalysis mechanism was shown in Fig. 7a. Firstly, the incorporation of GQDs enhanced the light-harvesting performance range from UV to NIR light, which is beneficial for generating more active electrons and holes on the surface of mesoporous Bi_2MoO_6. Secondly, the excellent electronic capture property of GQDs could perform as electron traps, which is beneficial for suppressing surface carrier recombination. Afterwards, the separated electrons will react with O_2 and H^+ and generate $\cdot O_2^-$ and H_2O_2, the H_2O_2 will quickly convert into ·OH by the chemical co-catalysis of GQDs (no photoelectrons are needed). On the other hand, the h^+ on the surface of the M-BM can oxidize the OH^- into ·OH. At last, the h^+, $\cdot O_2^-$ and ·OH can oxidize pollutants and achieve the degradation of pollutions.

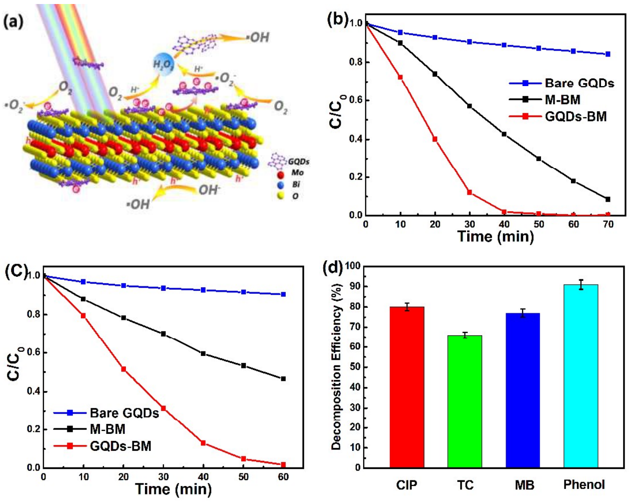

Fig. 7 Schematic representation of the photocatalysis mechanism (a); photocatalytic degradation of RhB (b) and BPA (c) in the presence of pure M-BM, GQDs-BM and GQDs under visible light irradiation; (d) photocatalytic decomposition efficiency of various pollutants using GQDs-BM as photocatalyst (within 30 min).

3.5.2 Photocatalytic activity and stability

The photooxidation performance before and after GQDs deposited were firstly evaluated by the degradation of RhB and BPA in the aqueous solution under the simulated sunlight. As presented in Fig. 7b, when using bare M-BM as photocatalyst, only 42% of RhB can be decomposed with 30 min. But, after the deposition of GQDs, nearly 90% of the RhB can be degraded within 30 min. Similarly, when using BPA as target pollutant (Fig. 7c), the GQDs-BM photocatalyst can decomposed 69% of the pollutants within 30 min, with is almost 2.3 times higher than bare M-BM. Moreover, as co-catalyst, the bare GQDs do not have obvious photocatalytic activity, but, the physical and chemical simultaneous co-catalysis of GQDs can effectively enhance the photocatalytic performance of mesoporous photocatalyst (M-BM). On the other hand, in order to generalize the effectiveness of our photocatalyst, we investigate the photocatalytic performance of GQDs-BM photocatalyst for degradation a diverse range of pollutants, such as MB, TC, CIP and phenol under simulated sunlight irradiation which shown in Fig. 7d. As results, the degradation of phenol exhibits the best effect, demonstrating the unique catalytic behavior under our experimental conditions.

The reusability and stability of photocatalysts are very important to the practical application. To evaluate the reusability and stability of GQDs-BM hybrid photocatalyst, recycling experiment are performed for the decomposition of BPA under simulated sunlight irradiation (Fig. S13a). After five cycles, the photoreactivity of GQDs-BM not found significant decrease, indicating this hybrid material with high stability. The XRD spectrum of GQDs-BM hybrid material before and after the photocatalytic reactions are shown in Fig. S13b, the crystal structures of the GQDs-BM nanocomposite is no obvious change. Moreover, the XPS spectrum and SEM images of GQDs-BM after photooxidation reactions can further ensure the stability of GQDs-BM hybrid photocatalyst (Fig S14).

4. Conclusion

In conclusion, we have presented a smart co-assembly strategy to incorporate ultrasmall (sub-3-nm) graphene quantum dots into the porous structure of mesoporous photocatalyst (M-BM) by a novel electrostatic self-assembly process. This strategy (ultrasmall 0D-sized material as co-catalyst, electrostatic self-assembly method) is also applicable to other mesoporous photocatalysts, which can make the modification material fully contact with the mesoporous photocatalyst and achieve the well-dispersed within the mesoporous structure. Besides that, the physical and chemical co-catalysis of GQDs, such as suppressing surface recombination, enhancing optical absorption ability from UV to NIR light and improving the utilization efficiency of photo-excited electrons, were systematically and comprehensively investigated. This co-catalysis of GQDs is favorable to a broad range of broad-spectrum photocatalysts, especially some photocatalysts which can only generate H_2O_2 by photoreduction, besides charge separation and optical absorption, the peroxidase-like activity of GQDs can enhance the utilization efficiency of photo-excited electrons for photooxidation in nature. At last, we believe, this work will provide a new idea for the skilled application of GQDs in the photocatalytic fields and paves an ingenious way to modify mesoporous photocatalysts.

Acknowledgements

This research was supported by the National Natural Science Foundation of China (Grant no. 21476033) and Cultivation Program for Excellent Talents of Science and Technology Department of Liaoning Province (no. 201402610).

View Article Online
DOI: 10.1039/C6TA02371A

References

1. A. Kudo, Y. Miseki, *Chem. Soc. Rev.,* 2009, 38, 253.
2. R. Asahi, T. Morikawa, T. Ohwaki, K. Aoki, Y. Taga, *Science.,* 2001, 293, 269-272.
3. W. X. Du, G. X. Yang, E. Wong, N. A. Deskins, A. I. Frenkel, D. Su, X. W. Teng, *J. Am. Chem. Soc*., 2014, 136, 10862.
4. J. W. Huang, Y. Ding, X. Luo, Y. Y. Feng, *J. Catal*., 2016, 333, 200.
5. Q. Xiang, J. Yu, J. Jaroniec, *Chem. Soc. Rev.,* 2012, 41, 782.
6. B. Liu, L. M. Liu, X. F. Lang, H. Y. Wang, X. W.(David). Lou, E. S. Aydil, *Energy Environ. Sci.*, 2014, 7, 2592.
7. C. C. Chen, W. H. Ma, J. C. Zhao, *Chem. Soc. Rev.,* 2010, 39, 4206.
8. Y. R. Wang, W. L. Yang, L. Zhang, Y. Hu, X. W. (David), *Nanoscale*, 2013, 5, 10864.
9. X. H. Gao, H. B. Wu, L. X. Zheng, Y. J. Zhong, Y. Hu, X. W. (David) Lou, *Angewandte Chemie-International Edition,* 2014, 23, 5197.
10. B. J. Jin, Z. B. Jiao, Y. P. Bi, *J. Mater. Chem. A.*, 2015, 3, 19702.
11. Y. Ma, Y. L. Jia, Z. B. Jiao, M. Yang, Y. X. Qi, Y. P. Bi, *Chem. Commun*., 2015, 51, 6655.
12. X. X. Yao, W. W. Wang. W. Chen, X. H. Liu, *Nanoscience: Volume 3.*, 2016, 3, 211.
13. Z. Dai, F. Qin, H. P. Zhao, F. Tian, Y. L. Liu, R. Chen, *Nanoscale*., 2015, 7, 11991.
14. G. H. Tian, Y. J. Chen, J. Zhou, C. H. Tian, R. Li, C. J. Wang, H. G. Fu, *CrystEngComm*., 2014, 16, 842.
15. M. Shang, W. Z. Wang, J. Ren, S. M. Sun, L. Zhang, *Nanoscale.*, 2011, 3, 1474.
16. Z. Luo, A. S. Poyraz, C. H. Kuo, R. Miao, Y. T. Meng, S. Y. Chen, T. Jiang, C. Wenos, S. L. Suib, *Chem. Mater.,* 2015, 27, 6.
17. X. D. Wang, L. Cao, D. H. Chen, R. A. Caruso, *ACS Appl. Mater. Interfaces.,* 2013, 5, 9421.
18. H. X. Li, Z. F. Bian, J. Zhu, D. Q. Zhang, G. S. Li, Y. N Huo, H. Li, Y. F. Lu, *J. Am. Chem. Soc.,* 2007, 129, 8406.
19. Y. Zhang, J. Li, Y. Wang, *Chem. Mater.*, 2006, 18, 2917.
20. W. Zhou, W. Li, J. Q. Wang, Y. Qu, Y. Yang, Y. Xie, K. F. Zhang, L. Wang, H. G. Fu, D. Y. Zhao, *J. Am. Chem. Soc.*, 2014, 136, 280.
21. W. Li, F. Wang, Y. P. Liu, J. X. Wang, J. P. Yang, L. J. Zhang, A. A. Elzatahry, D. Al-Dahyan, Y. Y. Xia, D. Y. Zhao, *Nano Lett*., 2015, 15, 2186.
22. M. K. Hossain, A. R. Koirala, U. S. Akhtar, M. K. Song, K. B. Yoon, *Chem. Mater.*, 2015, 27, 6550.
23. Z. C. Lian, P. P. Xu, W. C. Wang, D. Q. Zhang, S. N. Xiao, X. Li, G. S. Li, *ACS Appl. Mater. Interfaces.*, 2015, 7, 4533.
24. S. Sreejith, X. Ma, Y. L. Zhao, *J. Am. Chem. Soc.*, 2012, 134, 17346.
25. Y. Wang, K. T. Wang, J. F. Zhao, X. G. Liu, J. Bu, X. Y. Yan, R. Q. Huang, *J. Am. Chem. Soc.*, 2013, 135, 4799.
26. O. Mehraj, B. Pirzada, N. Mir, S. Sultana, S. Sabir, *RSC Adv*., 2015, 5, 42910.
27. F. X. Wang, L. Liang, L. Shi, M. H. Liu, J. M. Sun, *Dalton Trans*., 2014, 43, 16441.
28. L. Shi, L. Liang, J. Ma, F. X. Wang, J. M. Sun, *Dalton Trans*., 2014, 43, 7236.
29. C. Chang, L. Y. Zhu, S. F. Wang, X. L. Chu, L. F. Yue, *ACS Appl. Mater. Interfaces.*, 2014, 6, 5083.
30. N. Wu, J. Wang, D. N. Tafen, H. Wang, J. G. Zheng, J. P. Lewis, X. Liu, S. S. Leonard, A. Manivannan, *J. Am. Chem. Soc.*, 2010, 132, 6679.
31. P. V. Kamat, *J. Phys. Chem. Lett*., 2012, 3, 663.
32. Y. Xie, M. B. Teunis, B. Pandit, R. Sardar, J. Liu, *J. Phys. Chem. C.*, 2015, 119, 2813.
33. K. Tvrdy, P. A. Frantsuzov, P. V. Kamat, *Proc. Natl. Acad. Sci.*, 2011, 108, 29.
34. G. S. Li, D. Q. Zhang. J. C. Yu, *Chem. Mater.*, 2008, 20, 3983.
35. S. M. Sun, W. Z. Wang, J. H. Xu, L. Wang, Z. J. Zhang, *Applied Catalysis B: Environmental.*, 2011, 106, 559.
36. X. Zhao, W. J. Luo, J. Y. Feng, M. X. Li, Z. S. Li, T. Yu, Z. G. Zou, *Adv. Energy Mater.*, 2014, 4, 1301785.
37. T. W. Kim, K. S. Choi, *Science.,* 2014, 343, 990.
38. F. Shen, W. Que, Y. Liao, X. Yin, *Ind. Eng. Chem*., 2011, 50, 9131.
39. F. Dong, Q. Y. Li, Y. J. Sun, W. K. Ho, *ACS Catal*., 2014, 4, 4341.
40. J. Dai, J. X. Xia, M. X. Ji, H. P. Li, H. Xu, H. M. Li, R. Chen, *Nanoscale*., 2015, 7, 11433.
41. H. Li, J. Shang, Z. H. Ai, L. Z. Zhang, *J. Am. Chem. Soc.*, 2015, 137, 6393.
42. H. Xu, L. Z. Zhang, *J.Phys.Chem. C.*, 2010, 114, 940.
43. H. Wang, Y. Su, H. X. Zhao, H. T. Yu, S. Chen, Y. B. Zhang, X. Quan, *Environ. Sci. Technol.*, 2014, 48, 11984.
44. J. Y. Sheng, X. J. Li, Y. M. Xu, *ACS Catal.*, 2014, 4, 732.
45. M. Buzaglo, M. Shtein, O. Regev, *Chem. Mater.,* 2016, 28, 21.
46. B. S. Shen, J. W. Liang, R. S. Guo, X. Zhang, X. B. Yan, *ACS Appl. Mater. Interfaces.*, 2015, 7, 25378.
47. H. H. Cheng, Y. Zhao, Y. Q. Fan, X. J. Xie,L. T. Qu, G. Q. Shi, *ACS Nano.*, 2012, 6, 237.
48. Y. Li, Y. Zhao, H. H. Cheng, Y. Hu, G. Q. Shi, L. M. Dai, L. T. Qu, *J. Am. Chem. Soc.*, 2012, 134, 15.
49. Q. Lu, Y. J. Zhang, S. Q. Liu, *J. Mater. Chem. A*., 2015, 3, 8552.
50. H. J. Sunt, N. Gao, K. Dong, J. S. Ren, X. G. Qu, *ACS Nano.*, 2014, 8, 6202.
51. W. S. Hummers, R. E. Offeman, *J. Am. Chem. Soc*., 1958, 80, 1339.
52. Y. Hou, F. Zuo, Q. Ma, C. Wang, L. Bartels, P. Feng, *J. Phys. Chem. C.*, 2012, 116, 20132.
53. M. Y. Zhang, C. L. Shao, J. B. Mu, X. M. Huang, Z. Y. Zhang, Z. C. Guo, P. Zhang, Y. C. Liu, *J. Mater. Chem.*, 2012, 22, 577.
54. C. Y. Xu, Q. Han, Y. Zhao, L. X. Wang, Y. Li. L. T. Qu, *J. Mater. Chem. A.*, 2015, 3, 1841.
55. T. Yan, Q. Yan, X. D. Wang, H. Y. Liu, M. M. Li, S. X. Liu, W. G. Wu, M. Sun, *Dalton Trans.*, 2015, 44, 1601.
56. Y. H. Shin, J. T. Park, D. S. Hyun, J. H. Yang, H. Y. Lee, *New J. Chem*., 2015, 39, 2425.
57. Y. H. Shin, J. T. Park, D. S. Hyun, J. H. Yang, J. H. Lee, J. H. Kim, H. Y. Lee, *Nanoscale.*, 2015, 7, 5633.
58. M. Hassan, E. Haque, K. R. Reddy, A. I. Minett, J. Chenc, V. G. Gomes, *Nanoscale.*, 2014, 6, 11988.
59. Y. Zhang, H. Gao, J. J. Niu, B. T. Liu, *New J. Chem.*, 2014, 38, 4970.
60. Y. H. Zhu, G. F. Wang, H. Jiang, L. Chen, X. J. Zhang, *Chem. Commun.*, 2015, 51, 948.
61. J. Di, J. X. Xia, Y. P. Ge, H. P. Li, H. Y. Ji, H. Xu, Q. Zhang, H. M. Li, M. N. Li, *Applied Catalysis B: Environmental.*, 2015, 168-169, 51-61.
62. F. Dong, Z. W. Zhao, Y. J. Sun, Y. X. Zhang, S. Yan, Z. B. Wu, *Environ. Sci. Technol.*, 2015, 49, 12432.
63. H. C. Ma, L. X. Yue, C. L. Yu, X. L. Dong, X. X. Zhang, M. Xue, X. F. Zhang, Y. H. Fu, *J. Mater. Chem.*, 2012, 22, 23780.
64. Y. Hou, Z. H. Wen, S. M. Cui, X. R. Guo, J. H. Chen, *Adv. Mater.,* 2013, 25, 6291.
65. F. He, G. Chen, Y. G. Yu, S. Hao, Y. S. Zhou, Y. Zhang, *ACS Appl. Mater. Interfaces.*, 2014, 6, 7171.
66. F. Le. Formal, N. Tétreault, M. Cornuz, T. Moehl, M. Grätzel, K. Sivula, *Chem. Sci.*, 2011, 2, 737.
67. F. Le. Formal, K. Sivula, M. Gratzel, *J. Phys. Chem. C.*, 2012, 116, 26707.
68. J. L. Li, X. J. Liu, X. Q. Piao, Z. Sun, L. K. Pan, *RSC Adv*., 2015, 5,

View Article Online
DOI: 10.1039/C6TA02371A

16592.
69. J. Yang, X. H. Wang, X. L. Zhao, J. Dai, S. R. Mo, *J. Phys. Chem. C.*, 2015, 119, 3068.
70. R. Li, Z. J. Wang, L. Wang, B. C. Ma, S. Ghasimi, H. Lu, K. Landfester, K. A. I. Zhang, *ACS Catal.*, 2016, 6, 1113.
71. C. M. Li, G. Chen, J. X. Sun, J. C. Rao, Z. H. Han, Y. D. Hu, Y. S. Zhou, *ACS Appl. Mater. Interfaces.*, 2015, 7, 25716.
72. X. Q. Xiong, H. H. Chen, Y. M. Xu,*J. Phys. Chem. C.*, 2015, 119, 5946.
73. H. Zhang, L. H. Guo, L. X. Zhao, B. Wan, Y. Yang, *J. Phys. Chem. Lett.*, 2015, 6, 958.
74. H. X. Shi, G. X. Huang, D. H. Xia, T. W. Ng, H. Y. Yip, G. Y. Li, T. C. An, H. J. Zhao, P. K. Wong, *J. Phys. Chem. B.*, 2015, 119, 3104.
75. H. Bader, V. Sturzenegger, J. Hoigne´, *Water Res.,* 1988, 22, 1109.

View Article Online
DOI: 10.1039/C6TA02371A

TOC Graphic